*European Journal of Orthodontics*, 2020, 509–516
doi:10.1093/ejo/cjaa007
Advance Access publication 29 April 2020

Original article

# Three-dimensional changes in the craniofacial complex associated with soft-diet feeding

**Kana Kono[1], Chihiro Tanikawa[2], Yuka Murata[2], Takeshi Yanagita[1], Hiroshi Kamioka[1] and Takashi Yamashiro[2,]**

[1]Department of Orthodontics, Graduate School of Medicine, Dentistry and Pharmaceutical Sciences, Okayama University, Okayama, Japan, and [2]Department of Orthodontics and Dentofacial Orthopedics, Graduate School of Dentistry, Osaka University, Osaka, Japan

Correspondence to: Takashi Yamashiro, Department of Orthodontics and Dentofacial Orthopedics, Graduate School of Dentistry, Osaka University, Osaka, Japan. E-mail: yamashiro@dent.osaka-u.ac.jp

## Summary

**Background and objectives:** The masticatory force affects craniofacial development. We aimed to quantify the topological deviation of the growing craniofacial structure due to soft-food diet feeding and to map the region where the phenotypes appeared on three-dimensional (3D) images.
**Material and methods:** Mice were fed a powdered soft diet (SD) or conventional hard diet (HD) of regular rodent pellets at 3 weeks of age until 9 weeks of age. The heads, excluding the mandibles, were scanned by micro-computed tomography. The topographic deviation of the bony surface was quantitatively assessed by a wire mesh fitting analysis. The actual displacement and significant differences were mapped and visualized in each *x*-, *y*-, and *z*-axis on the 3D craniofacial image. On these reconstructed images, two-dimensional linear measurements between the landmark points confirmed the 3D skeletal displacement.
**Results:** In the transverse direction, the zygomatic arches and the region in which the temporal muscle attaches to the parietal and temporal bones were narrow in the SD group. The temporal muscle attachment regions significantly shifted anteriorly, and consequently, the sagittal zygomatic arch shortened. Although the cranial sagittal length was not affected, the vertical height was also reduced in the SD group compared to the HD group.
**Conclusions:** Our 3D surface-based analysis demonstrated that SD feeding resulted in reduced 3D bony development at the region where the chewing muscles attach to the zygomatic arches and the temporal and parietal bones. Interestingly, SD feeding induced an anterior shift in the temporal and parietal bone regions, which can affect the skeletal inter-jaw relationship.

## Introduction

Decreased masticatory stress associated with refined and soft food may contribute to the development of malocclusion. The craniofacial complex is composed of multiple bones with various morphologies, and the masticatory muscle directly attaches to the craniofacial bone surface (1). Masticatory loading is an important environmental factor that influences the craniofacial development (2), and a soft-food diet model is one animal experimental model used to evaluate how masticatory loading affects the craniofacial and dento-alveolar bone development (3–11).

The craniofacial morphology has been often evaluated by linear measurements between reference points at structures of interest using radiographs or by direct measurement. Although such two-dimensional (2D) analyses provide valuable information for understanding the morphological phenotypes in soft diet (SD) mice, 2D imaging is based on projecting the 'shadow' of hard tissues and can explain only a fraction of the three-dimensional (3D) changes in the complicated shapes of the craniofacial bones.

Such limitations have recently been overcome with the introduction of micro-computed tomography (CT), which enables the

capture of 3D images with high resolution and accuracy. However, 2D measurements are still performed on reconstructed slices or among reference points of 3D images, so 3D digital image data have not been efficiently used in many cases (7, 12–15).

We recently described the surface-based analysis of 3D data for quantifying and visualizing topological bone surface deviations (16). In that analysis, significant differences in the values at the *x*-, *y*-, and *z*-axis were mapped onto 3D images, thus enabling the mapping of bone surface regions with significant deviations on 3D images and consequently providing much more detailed information on the morphological phenotypes of the mandible than has previously been available.

Many studies using SD fed rats or mice have focussed on the development of the mandible, presumably due to its simple morphology (4, 5, 8–10, 13, 15, 17). Our 3D surface-based analysis clarified that the skeletal displacement due to SD feeding was most significant at the region of the inferior border of the mandible, where the masseter muscle attaches. These findings led us to suspect that the nasomaxillary regions, where the opposite end of the masseter masticatory muscle attaches, may also be affected by SD feeding. However, the previous evaluation of the maxillary phenotypes has been relatively limited. Indeed, the narrowing of the lateral dimension of the maxilla (18–21), anteriorly directed maxillary growth (4, 20, 22), and narrowing of the upper dental arches (19–21) have all been reported as nasomaxillary and dento-alveolar phenotypes in SD fed rats. The nasomaxillary regions are more complicated in shape than the limb bones, and the regions of masticatory muscle attachment cannot be easily traced or measured on 2D radiographs. Such technical difficulties have presumably hindered the detection of further effects of mastication on the nasomaxillary growth.

In the present study, we applied our surface-based analysis to investigate the effect of supposedly changed muscular function on the craniofacial and dento-alveolar growth.

## Materials and methods

All aspects of animal care and experiments were approved by the Okayama University Committee for Animal Care and Use. To minimize animal suffering, the number of animals used was based on the minimum required to obtain statistically valid results. An *a priori* power analysis was performed using our preliminary measurement outcomes with the R software program (R-project.org) and showed that a sample size of (6 per group) was deemed adequate to determine significant difference between groups (80% power, $\alpha = 0.05$, 2-sample *t*-test [1-sided]).

Three-dimensional surface images consisting of about 1 million points were extracted from micro-CT data of the mouse heads. High-resolution template meshes were then fitted onto the 3D surface images based on the assigned landmark to generate homogeneous models consisting of about 10.000 wire mesh points. Finally, the deviation in the coordinate values of each corresponding point on the wire mesh was calculated to generate colour maps representing the actual displacement and significance of differences between the control and experimental groups (Supplementary Figure 1), as described previously (16).

### Animals

Twelve ICR mice (CREA) at 3 weeks of age were randomly divided into groups receiving a hard diet (HD) and SD (Powder CE-2; CREA, Japan). The HD group was fed regular and solid rodent pellets (CE-2; CREA), and the SD group was fed powdered pellets with the same nutritional value until 9 weeks old. All animals were housed 3 or 4 to a cage, fed and watered *ad libitum* and maintained at 23 ± 1°C with a 12-hour day/night cycle.

### Micro-CT and generation of the 3D model

Micro-CT images were taken to reconstruct the anatomical 3D images. Mice were sacrificed at 9 weeks old, and the heads were fixed in 4% paraformaldehyde for 12 hours. Micro-CT images were taken with a Ratheta LCT-200 In Vivo Micro-CT Scanner for Small Lab Animals (HITACHI-Aloka, Tokyo, Japan) at 90 kV and 110 mA with a 96-μm slice width and 1-voxel size at 96 × 96 × 96 μm.

Surface generation from micro-CT data was performed with 3D Slicer (version 4.5.0-1, http://www.slicer.org) (23), which is an open-source software platform for the analysis and visualization of CT data. Following data preparation, semiautomatic segmentation was performed on this platform using a region-growing algorithm called GrowCut (Supplementary Figure 1).

### Reference plane for the 3D analysis

The definition of the reference plane directly influences the interpretation of the morphological changes associated with SD feeding. The reference plane and/or points should be stable, especially when growing experimental animals are used. The trigeminal nervous system develops early before the ossification of the craniofacial skeleton, making the position of the canal would be relatively stable. Therefore, the infraorbital foramen was selected as the point of origin for morphological comparison. In contrast, in our previous study, the occlusal plane was used to define the *x*–*z* plane in the superimposition of the 3D mandibular models (16). However, our preliminary study found that the vertical displacement between the calvaria and upper occlusal plane was significantly more pronounced in the M3 regions than in the M1 regions, indicating that the upper occlusal plane is not stable as a reference plane for the evaluation of the craniofacial complex. If the 3D images were superimposed based on the occlusal plane, the downward rotation of the reference plane would be recognized as the head orientation changed, affecting the vertical and anterior–posterior location of the landmarks in the present coordinate system and subsequent analyses of the displacement. Therefore, we defined our reference plane as the plane parallel to the nasal floor plane at the infraorbital foramen. The nasal floor plane was defined by bilateral reference points on incisive bone, resulting in the maxilla bone and this plane being less strongly influenced by mastication activity because no masticatory muscle attaches around the reference points. Using this reference plane, we confirmed that molar vertical displacement was appropriately evaluated, as the linear measurement data indicated.

### Coordinate system for the 3D analysis

We developed a coordinate system for the 3D analysis. The *x*–*z* plane was defined as the plane parallel to the nasal floor plane, from the midpoint of the bilateral infraorbital foramen. The *z*-axis was parallel and the *x*-axis perpendicular to the midline of the nasal floor plane on the *x*–*z* plane. The *y*-axis was perpendicular to the *x*–*z* plane at the midpoint of the bilateral infraorbital foramen.

### Identification of the landmarks and data processing

The positions of 82 landmarks (Supplementary Figure 2) were identified by a visual inspection of the image and digitized using a computer mouse cursor and shape analysis software program (HBM-Rugle; Medic Engineering Co., Kyoto, Japan). The 3D images were imported into the new coordinate system for standardization based on the aforementioned landmarks (Supplementary Figure 2).

For the homogeneous modelling, a high-resolution template wire mesh was fitted for each model using the HBM-Rugle software program, based on the landmarks assigned to each 3D image. Each homogeneous model consists of 6864 points (i.e. nodes of the fitted mesh) on the mesh, which facilitate a quantitative assessment of the topological deviation. This process extracts the relevant surface anatomy from micro-CT data, yielding high-resolution 3D surface data. The average distance between the points on the mesh was 32 ± 24 µm, which is less than the slice thickness of 96 µm. Thus, the mesh resolution employed was considered adequate for representing the original skull shape. The averaged 3D images were computed by the arithmetic means of the coordinate values of each corresponding point on the wire mesh for each group.

The surface displacement was quantitatively evaluated in each *x*-, *y*-, and *z*-axis in two different ways, as described before (16). The actual displacement and significance of differences were calculated on each mesh between the HD and SD groups. The calculated values in millimetres were visualized with colour-coding on the computed 3D models of HD mice. Thereafter, the arithmetic means of the coordinate values of each corresponding point on the wire mesh were statistically analysed for significant differences between the HD and SD groups using a two-sample *t*-test. A significance probability map (24) of the *x*-, *y*-, and *z*-values was generated to visualize these significant differences.

To confirm the morphological changes, we performed linear measurement between the defined reference points on the bone surface (Supplementary Figure 3).

## Results

### Averaged 3D images of the maxillary bones and the actual deviation

The averaged maxillary bone surface was computed for the SD (yellow in Supplementary Figure 1) and HD groups (blue in Supplementary Figure 1) and superimposed at the infraorbital foramen parallel to the occlusal plane (Supplementary Figure 1).

### Mapping of the actual displacement and the significant differences in the *x*-axis

The actual displacement and the significance probability map in the *x*-axis demonstrated that the whole bodies of the zygomatic arches, where the masseter muscles attach, were significantly displaced in the inward direction in the SD group (Figures 1 and 2). Interestingly, the significantly displaced region was further extended posteriorly to the temporal and parietal bone regions where the medial temporalis muscles attach. Such regions were also evident at the anterior part of the frontal bone. Direct linear measurements confirmed a decreased transverse width of the zygomatic arches (#4 and #5 in Supplementary Figure 3), the temporal bone (#6), but not the frontal bone (#3) (Figure 7).

### Mapping of the actual displacement and the significant differences in the *y*-axis

The actual displacement and the significance probability map in the *y*-axis demonstrated that the zygomatic arches were significantly displaced in the upward direction in SD mice (Figures 3 and 4). The upper incisors and the surrounding premaxilla regions were also displaced upward, indicating anterior growth in the SD mice. Significant vertical displacement was also confirmed by a decreased height between the maxillary molars and the calvaria bone. The shape changes associated with SD feeding were least prominently

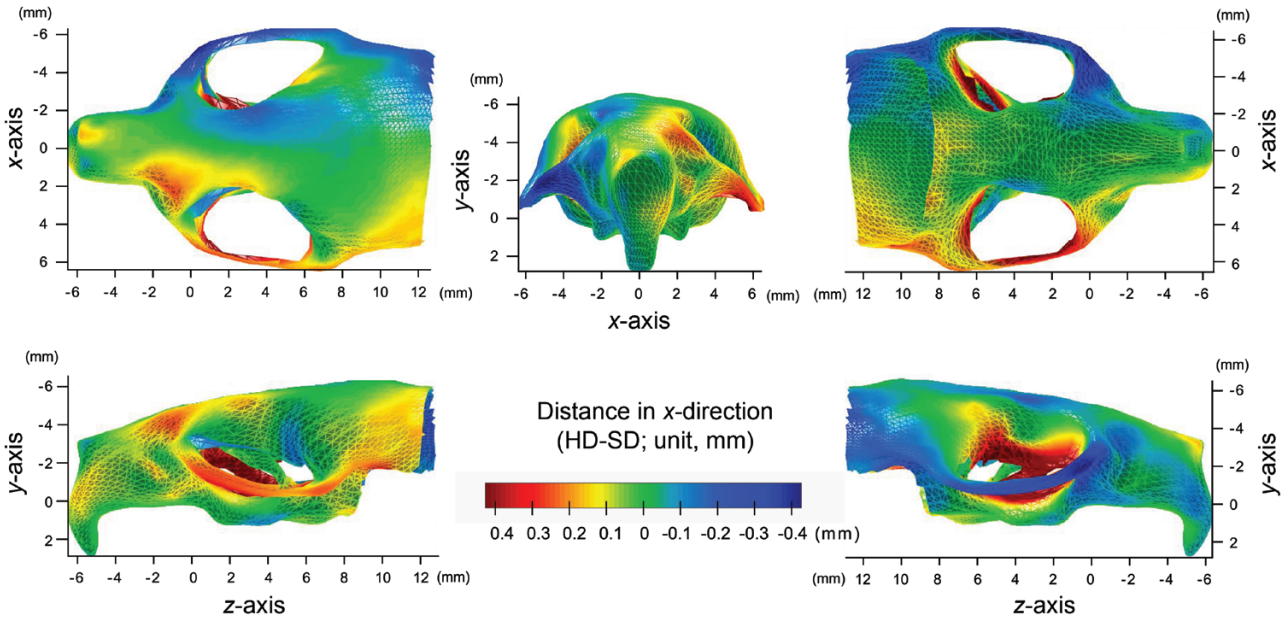


**Figure 1.** Actual displacement on each wire-mesh point in the x-axis. The heat map depicts positive (red) or negative (green) transverse displacement in SD mice compared with HD mice. The *x*–*z* plane was defined as the plane parallel to the nasal floor plane, from the midpoint of the bilateral infraorbital foramen. The *z*-axis was parallel and the *x*-axis perpendicular to the midline of the nasal floor plane on the *x*–*z* plane. The *y*-axis was perpendicular to the *x*–*z*plane at the midpoint of the bilateral infraorbital foramen. The top left indicates the superior view; top middle, frontal view; top right, inferior view; bottom left, left lateral view; bottom right, right lateral view of the craniofacial complex.

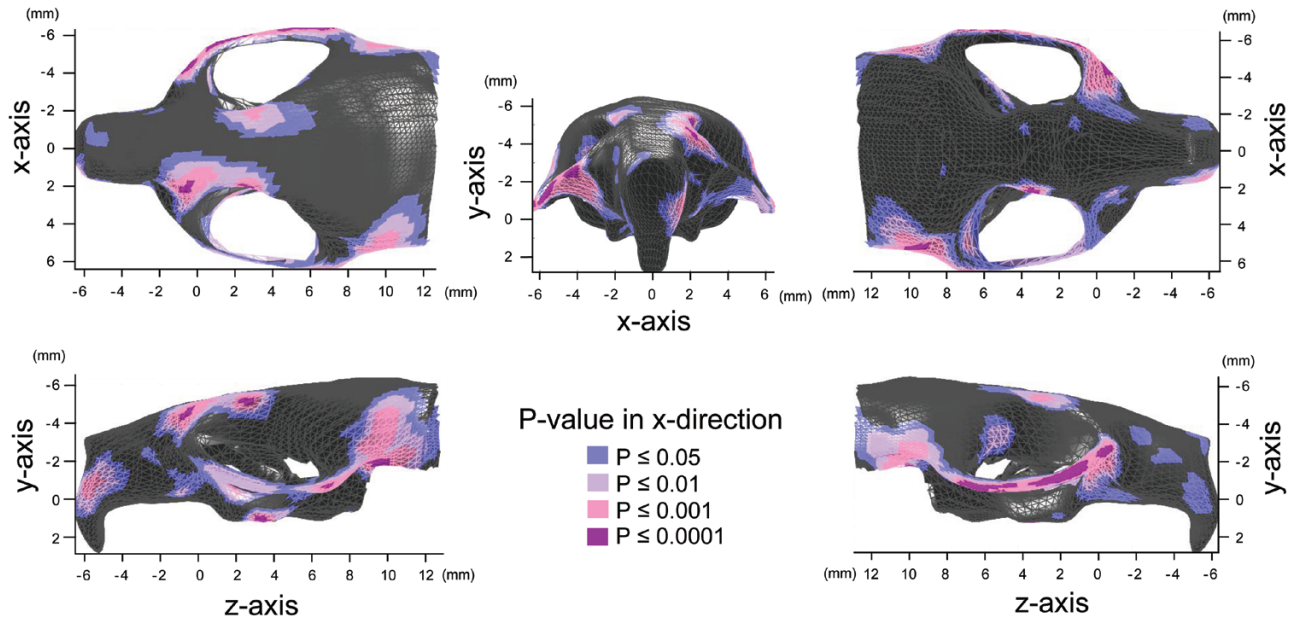


**Figure 2.** Significance probability map in the *x*-axis. Blue designates $P \leq 0.05$; pale pink, $P \leq 0.01$; dark pink, $P \leq 0.001$; purple, $P \leq 0.0001$.

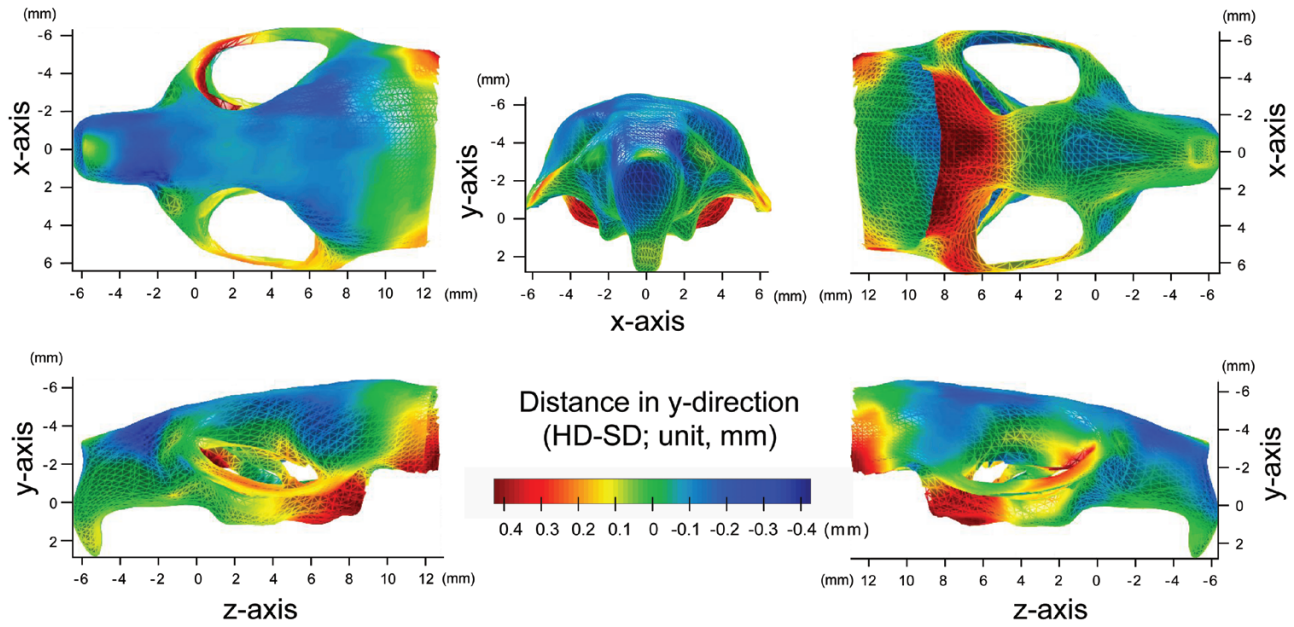


**Figure 3.** Actual displacement on each wire-mesh point in the *y*-axis. The heat map depicts positive (red) or negative (green) vertical displacement in SD mice compared with HD mice.

observed in the *y*-axis among the three dimensions (Figure 4 and Table 1). Direct linear measurements confirmed a decreased vertical distance between the calvaria and the zygomatic arches (#11 and #13 in Supplementary Figure 3). Significant reduction in the distance was also observed between the calvaria and the third molars (#12), but not between the calvaria and the first molars (#10) (Figure 7).

### Mapping of the actual displacement and the significant differences in the *z*-axis

The significance probability map in the *z*-axis demonstrated that the anterior surface of the maxillary bone was displaced in the posterior direction in SD mice, while the posterior part of the zygomatic arches and temporal bone regions was significantly displaced in the anterior direction in SD mice (Figures 5 and 6). Linear measurement confirmed a decreased anteroposterior (AP) length of the zygomatic arches (#17 and #19 in Supplementary Figure 3) and a decreased AP distance between the inferior orbital foramen and the temporal and parietal bones (#18). The AP lengths of the calvarial bones were not affected (#14–16) (Figure 7).

## Discussion

A soft-food diet is an established experiment model for understanding how masticatory loading affects the craniofacial growth

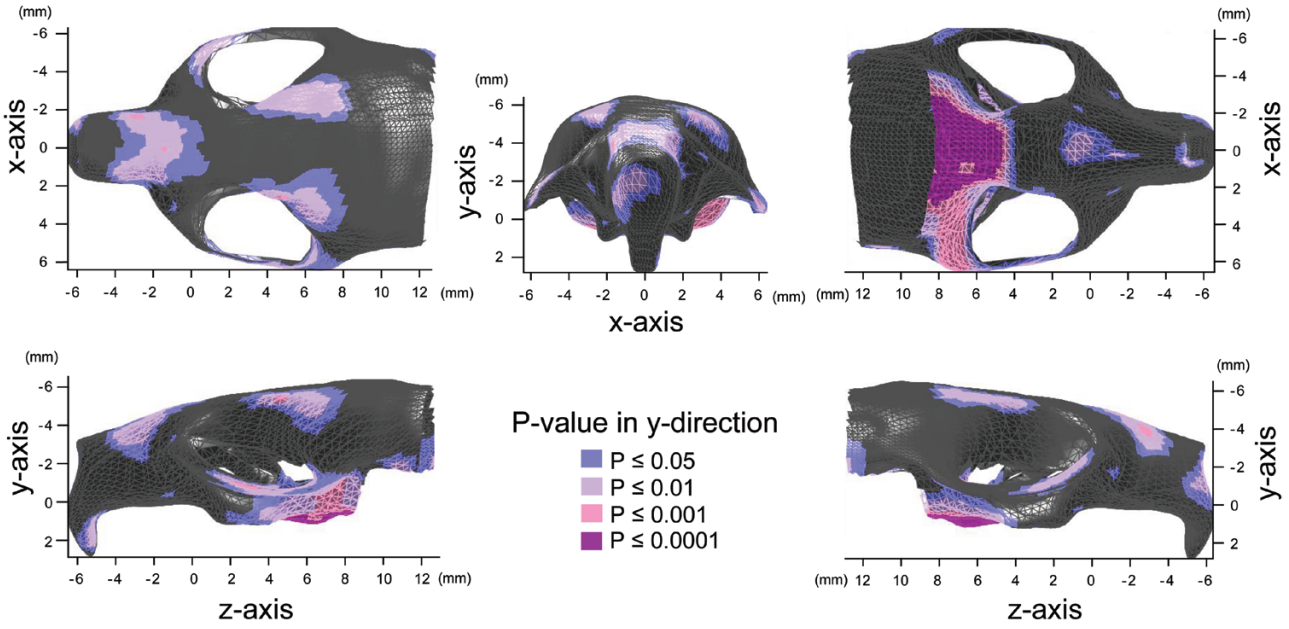


**Figure 4.** Significance probability map in the *y*-axis. Blue designates $P \leq 0.05$; pale pink, $P \leq 0.01$; dark pink, $P \leq 0.001$; purple, $P \leq 0.0001$.

**Table 1.** Result summary of linear measurement.

| # | Measurements | Points | HD group (mm) | | SD group (mm) | | *P* |
|---|---|---|---|---|---|---|---|
| | | | Mean | SD | Mean | SD | |
| 1 | The width between the anterior notch on zygomatic plate | 15-34 | 5.797 | 0.121 | 5.947 | 0.153 | - |
| 2 | The Anterior (Superior)width between the superior and lateral intesection of zygomatic process and zygomatic arch | 19-38 | 9.714 | 0.277 | 9.427 | 0.327 | - |
| 3 | The Anterior width between the innermost and highest point of frontal bones | 45-46 | 3.728 | 0.060 | 3.154 | 1.069 | - |
| 4 | The width between the intersection of zygomatic process of maxilla with zygoma, superior surface | 64-65 | 11.776 | 0.280 | 11.211 | 0.121 | ↓↓ |
| 5 | The width between the intersection of zygoma with zygomatic process of temparal, superior aspect | 22-41 | 12.655 | 0.212 | 12.203 | 0.115 | ↓↓ |
| 6 | The width between the posterior zygomatic root connecting squamosal body | 25-44 | 10.911 | 0.071 | 10.590 | 0.115 | ↓↓ |
| 7 | The width between the most mesial point of M1 | 31-10 | 4.004 | 0.089 | 3.900 | 0.114 | - |
| 8 | The width between the most distal point of M3 | 32-11 | 4.078 | 0.076 | 4.210 | 0.053 | ↓↓ |
| 9 | The distance between the Nasion and the midpoint of superior and lateral intesection of zygomatic process and zygomatic arch | 2-19, 38 | 2.733 | 0.112 | 2.604 | 0.156 | - |
| 10 | The distance between the innermost and highest point of frontal bones and the most mesial point of M1 (L) | 45-10 | 6.458 | 0.114 | 6.451 | 0.121 | - |
| 11 | The distance between the intersection of zygomatic process of maxilla with zygoma, superior surface and the midpoint of the Nasion and the Bregma | 2, 3-64, 65 | 4.786 | 0.059 | 4.569 | 0.133 | ↓↓ |
| 12 | The distance between the midpoint of the intersection of frontal and squamosal bones at temporal crest and the midpoint of most distal point of M3 | 32, 11-79, 80 | 6.631 | 0.067 | 6.344 | 0.090 | ↓↓ |
| 13 | The distance between the Bregma and the midpoint of intersection of zygoma with zygomatic process of temparal, superior aspect | 3-22, 41 | 5.390 | 0.113 | 5.225 | 0.140 | ↓ |
| 14 | The distance between the Nasion and the Bregma | 2-3 | 6.574 | 0.108 | 6.554 | 0.145 | - |
| 15 | The distance between the Nasion and the intersection of parietal bones with anterior aspect of interparietal bone at midline | 2-4 | 11.210 | 0.672 | 10.921 | 0.163 | - |
| 16 | The distance between the Bregma and the intersection of parietal bones with anterior aspect of interparietal bone at midline | 3-4 | 4.439 | 0.105 | 4.396 | 0.172 | - |
| 17 | The distance between the anterior notch on zygomatic process and the the posterior zygomatic root connecting squamosal body (L) | 14-25 | 11.626 | 0.306 | 10.875 | 0.228 | ↓↓ |
| 18 | The distance between the posterior zygomatic root connecting squamosal body and the infraorbital foramen (L) | 25-82 | 12.588 | 0.205 | 12.250 | 0.160 | ↓↓ |
| 19 | The distance between the intersection of zygoma with zygomatic process of temparal, inferior aspect and the infraorbital foramen (L) | 23-82 | 10.444 | 0.202 | 10.174 | 0.245 | ↓ |
| 20 | The distance between the intersection of maxilla and premaxilla bone at mid-sagittal plane and the PNS | 9-12 | 6.558 | 0.171 | 6.245 | 0.241 | - |

↓↓, $P \leq 0.01$; ↓, $P \leq 0.05$; -, $P > 0.05$

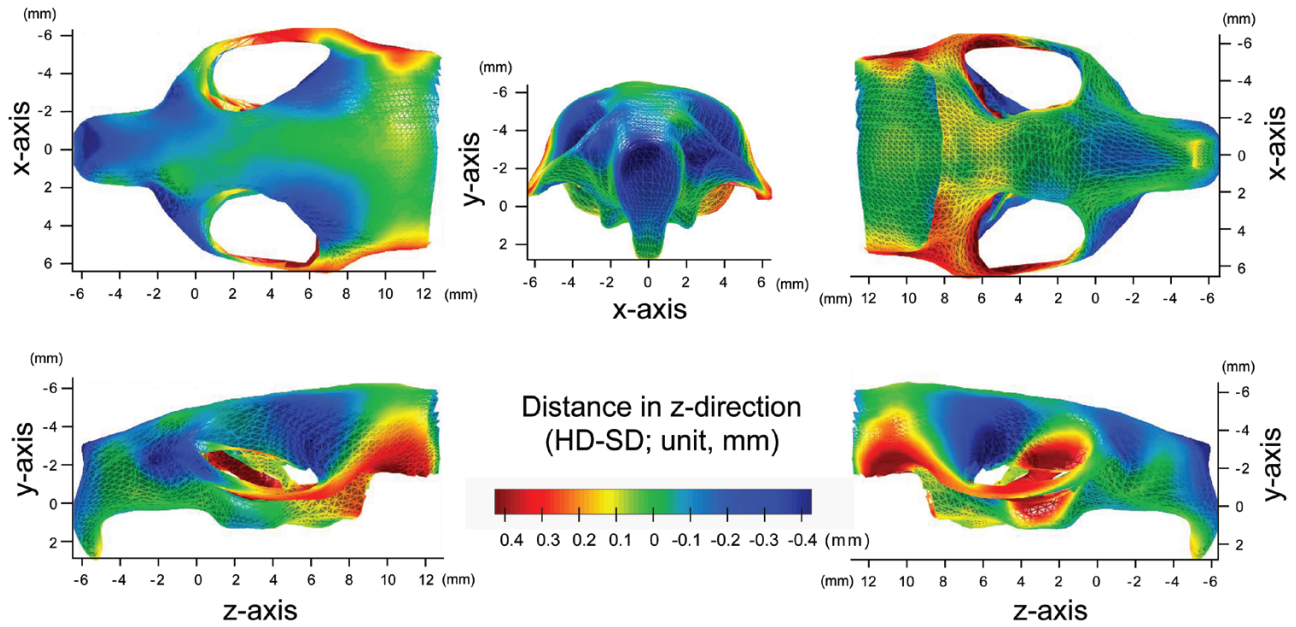


**Figure 5.** Actual displacement on each wire-mesh point in the *z*-axis. The heat map depicts positive (red) or negative (green) anterior–posterior displacement in SD mice compared with HD mice.

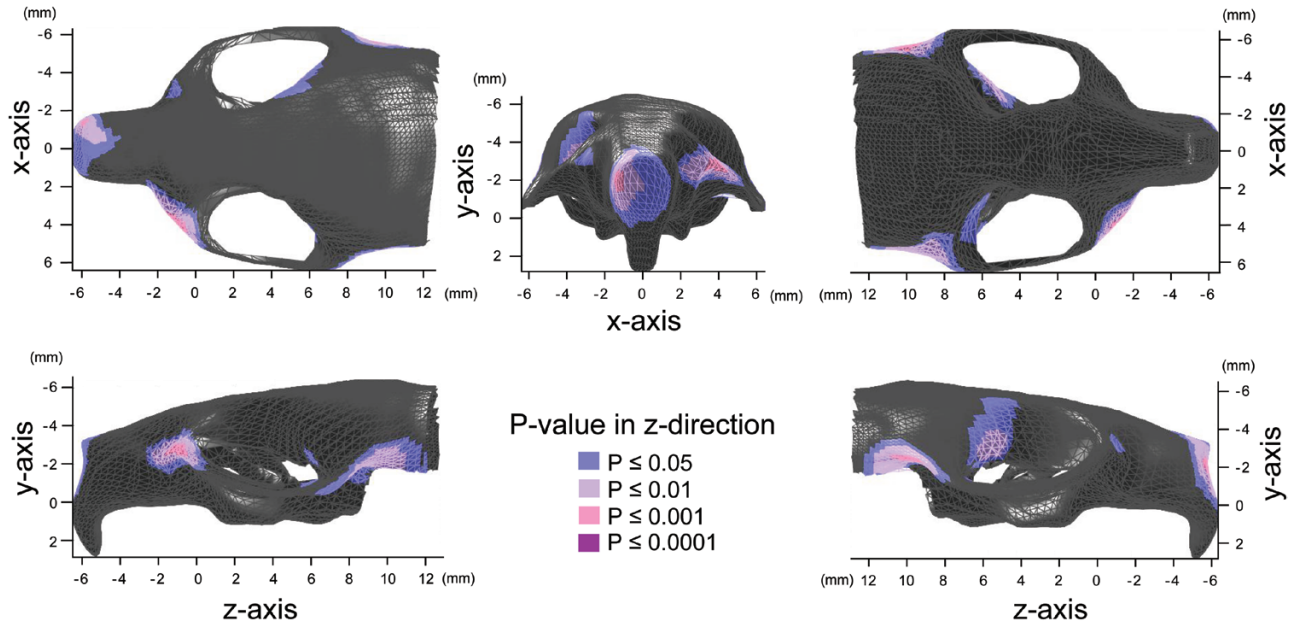


**Figure 6.** Significance probability map in the *z*-axis. Blue designates $P \leq 0.05$; pale pink, $P \leq 0.01$; dark pink, $P \leq 0.001$; purple, $P \leq 0.0001$.

and providing fundamental information about the possible association between human malocclusion and mastication (3–11). The bone growth of the cranial and nasomaxillary complex mainly occurs at the suture and the bone surface, and the masticatory muscle attaches to the facial bone surface with a unique characteristic distribution (25). It was therefore interesting to explore the effect of supposedly changed muscular function on the craniofacial growth and observe the possible topological association between the attachment of the muscle and the region of bony deviation. However, the maxillary bones have unique and complicated shape, and previous 2D cephalometric evaluations have been limited in detection of the bony deviation associated with a soft-food diet. This study was the first to conduct a bone surface analysis for the 3D evaluation (16) of micro CT data in the maxillary bone complex of SD mice.

The masseter muscle attaches to the zygomatic arch (26). Previous studies have demonstrated that SD feeding for 21 or 27 weeks results in a significant reduction in the transverse zygomatic arch width at the anterior regions of the zygomatic arch, but not at the middle (9). However, other studies using mice noted no such significant reduction in the zygomatic width (18–20, 22). Such discrepancies may be due to variations in experimental design, and a sufficient duration of SD feeding may be necessary to detect the relevant phenotype.

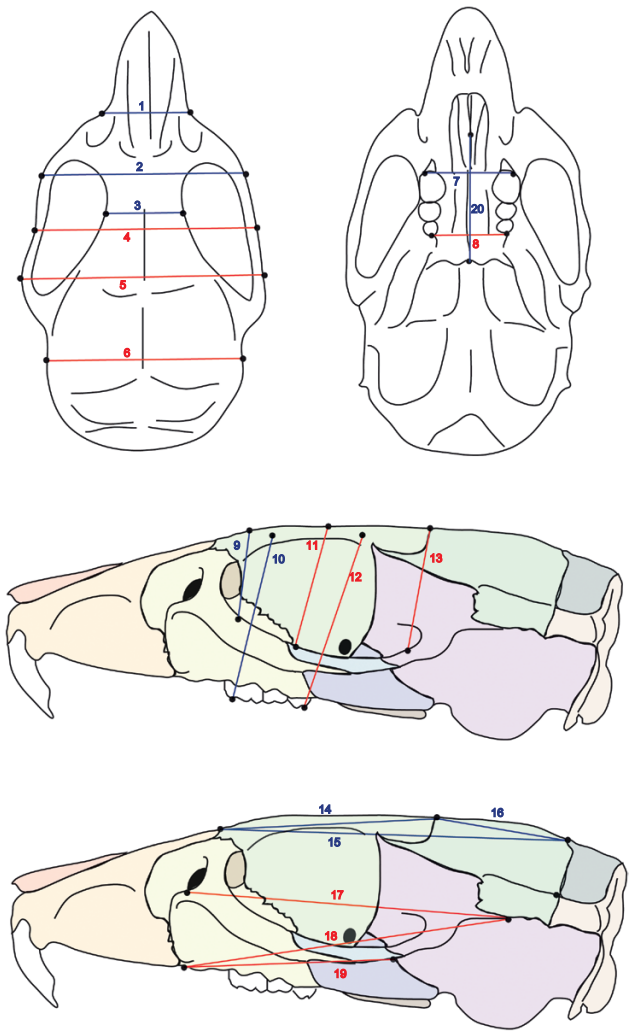


**Figure 7.** Diagram of direct linear measurement. Red indicates significant differences, while blue indicates no significant differences.

However, even though the duration of the SD feeding was relatively short in our present study, a 3D surface-based analysis was able to detect a significant reduction in the arch width, and our analysis clearly demonstrated that the whole surface of the zygomatic arch was significantly narrowed by SD feeding for 6 weeks, presumably due to our application of a highly accurate 3D surface-based analysis using micro-CT.

The region with significant inward deviation at the zygomatic arch further extended posteriorly on the temporal and parietal bones, which serve as attachment sites for the temporal muscles. Such changes were not demonstrated in previous studies using rats or mice. However, a longer duration of SD feeding for 6 months resulted in significant narrowing of the inter-parietal bone in ferrets, which are carnivores and not rodents (27). but not in rats or mice. In that study, however, SD was given for much longer than in the present study (6 months). The inter-temporal and intra-parietal widths were not evaluated in that study, presumably because reference points for the measurement of those bones are not easy to define accurately.

The significant difference map in the present study clearly mapped the regions of significant deviation and showed that these regions overlapped with the area of the temporal muscle attachment. In addition, the present 3D surface analysis was able to detect the SD-induced bony surface deviation with a much shorter duration of SD feeding than the 2D cephalometric analysis.

Interestingly. the region of the temporalis muscle attachment at the temporal and parietal bone surface shifted significantly in the forward direction (Figure 6). Indeed, our linear measurement confirmed the decreases in the distance between the temporal bone and the infraorbital foramen in SD mice (Figure 7). The temporal bone contains a glenoid fossa that envelopes the mandibular condyle; anterior shift of the temporal bone may thus imply that the mandible consequently was forced to be positioned more anteriorly. The anterior–posterior changes in the temporal or parietal bone had not been explored in 2D cephalometric analyses. These findings suggested that mastication problems in the temporal muscle might induce anterior positioning of the mandible.

The present significant difference map detected the significant upward deviation of the zygomatic arches in SD mice. Since the craniofacial growth is mainly in the anterior–inferior direction when the growth is evaluated based on the cranial base, our findings also indicate that the vertical growth of the zygomatic arch was disturbed more by SD feeding than the maxillary reference plane. Indeed, the linear measurement confirmed the reduction in the vertical height between the zygomatic and calvarial landmarks. Vertical changes in the zygomatic arches had not been shown before in 2D cephalometric analyses. On 2D lateral radiograph images, the shape of the zygomatic arch and other nasomaxillary complex bones are complicated with overlapping; therefore, linear measurements of the vertical dimension likely have large errors for detecting differences. Our surface-based analysis using high-resolution 3D images resolved these issues.

Our study has several limitations. In our experimental protocol, the internal structure of the cranial base structures can be visualized; however, only the bony surface information was evaluated. The internal structure of the cranial base structures might be able to be used for the stable reference plane both in animal studies and human cone beam computed tomography studies. We need to further explore the possible reference plane in the evaluation of the bony deviation associated with SD feeding.

In our present study, the maxillary dental arch width was not affected in the M1 regions but was widened in the M3 regions; a previous study, by contrast, demonstrated that the maxillary dental arch narrowed in SD animals (19–21). This discrepancy may be due to differences in the duration of SD feeding. What happens to the transverse width of the dento-alveolar regions if the duration of SD feeding is prolonged should be explored in a future study.

## Conclusions

We used our surface-based analysis to map the bone surface regions demonstrating significant topological deviation due to a soft-food diet and found that the craniofacial growth was significantly affected at the masticatory muscle attachment sites on the zygomatic arches and at the temporal and parietal bone regions.

## Supplementary material

Supplementary data are available at *European Journal of Orthodontics* online.

Supplementary Figure 1. Schematic illustration of the analyses employed in the present study.

Supplementary Figure 2. Landmarks on the craniofacial 3D images and the description.

Supplementary Figure 3. Diagram of the mouse skull with landmarks used for linear measurements and its description.

Supplemental Video 1. Significance probability map in the *x*-axis. *P* values were mapped on the averaged HD images.

Supplemental Video 2. Significance probability map in the *y*-axis on the averaged HD images. *P* values were mapped on the averaged HD images.

Supplemental Video 3. Significance probability map in the *z*-axis on the averaged HD images. *P* values were mapped on the averaged HD images.

## Funding

The present study was partially supported by Grant-in-Aid for Scientific Research from Japan Society for the Promotion of Science (17K17325 and 24792284).

## Conflicts of interest

None to declare.

## References

1. Larsson, E., Øgaard, B., Lindsten, R., Holmgren, N., Brattberg, M. and Brattberg, L. (2005) Craniofacial and dentofacial development in pigs fed soft and hard diets. *American Journal of Orthodontics and Dentofacial Orthopedics*, 128, 731–739.
2. Klingenberg, C.P. and Leamy, L.J. (2001) Quantitative genetics of geometric shape in the mouse mandible. *Evolution*, 55, 2342–2352.
3. Bouvier, M. and Hylander, W.L. (1984) The effect of dietary consistency on gross and histologic morphology in the craniofacial region of young rats. *The American Journal of Anatomy*, 170, 117–126.
4. Kiliaridis, S., Engström, C. and Thilander, B. (1985) The relationship between masticatory function and craniofacial morphology. I. A cephalometric longitudinal analysis in the growing rat fed a soft diet. *European Journal of Orthodontics*, 7, 273–283.
5. Kiliaridis, S., Thilander, B., Kjellberg, H., Topouzelis, N. and Zafiriadis, A. (1999) Effect of low masticatory function on condylar growth: a morphometric study in the rat. *American Journal of Orthodontics and Dentofacial Orthopedics*, 116, 121–125.
6. Maki, K., Nishioka, T., Shioiri, E., Takahashi, T. and Kimura, M. (2002) Effects of dietary consistency on the mandible of rats at the growth stage: computed X-ray densitometric and cephalometric analysis. *The Angle Orthodontist*, 72, 468–475.
7. Mavropoulos, A., Kiliaridis, S., Bresin, A. and Ammann, P. (2004) Effect of different masticatory functional and mechanical demands on the structural adaptation of the mandibular alveolar bone in young growing rats. *Bone*, 35, 191–197.
8. Kiliaridis, S. (2006) The importance of masticatory muscle function in dentofacial growth. *Seminars in Orthodontics*, 12, 110–119.
9. Odman, A., Mavropoulos, A. and Kiliaridis, S. (2008) Do masticatory functional changes influence the mandibular morphology in adult rats. *Archives of Oral Biology*, 53, 1149–1154.
10. Denes, B.J., Mavropoulos, A., Bresin, A. and Kiliaridis, S. (2013) Influence of masticatory hypofunction on the alveolar bone and the molar periodontal ligament space in the rat maxilla. *European Journal of Oral Sciences*, 121, 532–537.
11. Anderson, P.S., Renaud, S. and Rayfield, E.J. (2014) Adaptive plasticity in the mouse mandible. *BMC Evolutionary Biology*, 14, 85.
12. Swain, M.V. and Xue, J. (2009) State of the art of Micro-CT applications in dental research. *International Journal of Oral Science*, 1, 177–188.
13. Enomoto, A., Watahiki, J., Yamaguchi, T., Irie, T., Tachikawa, T. and Maki, K. (2010) Effects of mastication on mandibular growth evaluated by microcomputed tomography. *European Journal of Orthodontics*, 32, 66–70.
14. Saito, F., Kajii, T.S., Sugawara-Kato, Y., Tsukamoto, Y., Arai, Y., Hirabayashi, Y., Fujimori, O. and Iida, J. (2011) Morphological evaluation of cranial and maxillary shape differences of the brachymorphic mouse with spontaneous malocclusion using three-dimensional micro-computed tomography. *Orthodontics & Craniofacial Research*, 14, 100–106.
15. Goto, S., Fujita, Y., Hotta, M., Sugiyama, A. and Maki, K. (2015) Influence of differences in the hardness and calcium content of diets on the growth of craniofacial bone in rats. *The Angle Orthodontist*, 85, 969–979.
16. Kono, K., Tanikawa, C., Yanagita, T., Kamioka, H. and Yamashiro, T. (2017) A novel method to detect 3d mandibular changes related to soft-diet feeding. *Frontiers in Physiology*, 8, 567.
17. Nakano, H., Watahiki, J., Kubota, M., Maki, K., Shibasaki, Y., Hatcher, D. and Miller, A.J. (2003) Micro X-ray computed tomography analysis for the evaluation of asymmetrical condylar growth in the rat. *Orthodontics & Craniofacial Research*, 6(Suppl 1), 168–72; discussion 179.
18. Abed, G.S., Buschang, P.H., Taylor, R. and Hinton, R.J. (2007) Maturational and functional related differences in rat craniofacial growth. *Archives of Oral Biology*, 52, 1018–1025.
19. Katsaros, C., Berg, R. and Kiliaridis, S. (2002) Influence of masticatory muscle function on transverse skull dimensions in the growing rat. *Journal of Orofacial Orthopedics*, 63, 5–13.
20. Ulgen, M., Baran, S., Kaya, H. and Karadede, I. (1997) The influence of the masticatory hypofunction on the craniofacial growth and development in rats. *American Journal of Orthodontics and Dentofacial Orthopedics*, 111, 189–198.
21. Yamamoto, S. (1996) The effects of food consistency on maxillary growth in rats. *European Journal of Orthodontics*, 18, 601–615.
22. Tsai, C.Y., Yang, L.Y., Chen, K.T. and Chiu, W.C. (2010) The influence of masticatory hypofunction on developing rat craniofacial structure. *International Journal of Oral and Maxillofacial Surgery*, 39, 593–598.
23. Fedorov, A., et al. (2012) 3D Slicer as an image computing platform for the Quantitative Imaging Network. *Magnetic Resonance Imaging*, 30, 1323–1341.
24. Duffy, F.H., Bartels, P.H. and Burchfiel, J.L. (1981) Significance probability mapping: an aid in the topographic analysis of brain electrical activity. *Electroencephalography and Clinical Neurophysiology*, 51, 455–462.
25. Thilander, B. (1995) Basic mechanisms in craniofacial growth. *Acta Odontologica Scandinavica*, 53, 144–151.
26. Cox, P.G., Rayfield, E.J., Fagan, M.J., Herrel, A., Pataky, T.C. and Jeffery, N. (2012) Functional evolution of the feeding system in rodents. *PLoS One*, 7, e36299.
27. He, T. and Kiliaridis, S. (2003) Effects of masticatory muscle function on craniofacial morphology in growing ferrets (*Mustela putorius furo*). *European Journal of Oral Sciences*, 111, 510–517.